LA-UR-19-29657
Approved for public release; distribution is unlimited.

Title: Delayed Gamma Signature Accounting for Field Line Transport of Debris Ions after a Nuclear Explosion

Author(s): Mesick, Katherine Elizabeth

Intended for: Report

Issued: 2019-09-25

LA-UR-XX-XXXXX

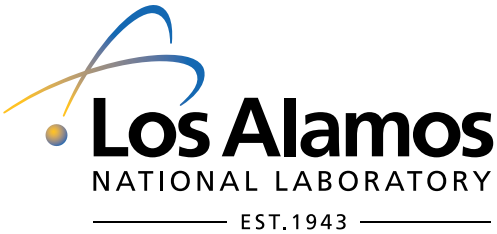

Delayed Gamma Signature Accounting for Field Line Transport of Debris Ions after a Nuclear Explosion

Katherine E. Mesick
Space Science and Applications, ISR-1
Los Alamos National Laboratory
kmesick@lanl.gov

September 19, 2019

Contents

1 Overview

Delayed gammas (DGs) are produced by the decay of radioactive fission fragments after a nuclear explosion. Currently, the time and energy profile of the delayed gamma signal is propagated in DIORAMA to the GEO satellite sensors by assuming a point source at the burst location for the production of the delayed gammas [1]. However, in reality the production of delayed gammas is spread over some spatial extent. First, the debris ions are confined within an expanding region by the magnetic field and/or surrounding plasma. This expanding confinement bubble eventually collapses, at which point the debris ions can be trapped on magnetic field lines and transported away from the original burst location [2, 3].

In this work the effects of debris ion transport on the associated time profile of delayed gammas at a GEO satellite is presented. The first step was the development of the Delayed Gamma Source Model (DGSM), which is based on the analytical Electron Source Model (ESM) code developed at LANL [4] that models the spatial distribution of energetic electrons produced after a high-altitude nuclear explosion (HANE) for use as a source term in LANL artificial belt diffusion code. This model creates a spatial grid in latitude, longitude, and altitude of the distribution of radioactive debris ions. The output of this code is combined with a separate analysis code also described, which produces the DG time profile signature at a GEO sensor faceplate when accounting for the spatial spread of delayed gamma production during field line transport. Some simple case studies are presented to show how the DG signature at GEO calculated with this higher-fidelity model and a simple point-source model, as is currently assumed in DIORAMA, compare.

2 Delayed Gamma Source Model

The Delayed Gamma Source Model (DGSM) was developed for this study by making a few modifications to the ESM code in existence[1]. More details of the ESM model can be found in [4], but several of the input parameters, models, and assumptions are summarized below for completeness within the context of the DGSM. Many of these descriptions come from [4].

An example of the input csv file that is passed when running the code is shown in the Appendix. The DGSM takes the following input parameters, and some of these are described in more detail below within the context of the DGSM models, assumptions, and limitations.

DGSM_Date: Date of burst
DGSM_Time: Time of burst
DGSM_GeodLat: Geodetic latitude of burst, °N
DGSM_GeodLong: Geodetic longitude of burst, °E
DGSM_GeodHeight: Geodetic altitude of burst, km
DGSM_Yb: Yield of burst, kT
DGSM_AtmGeodHeight: Geodetic height of atmosphere cutoff, km
DGSM_haa: Global atmosphere cutoff to mimic drift loss cone, km
DGSM_Ud: Thermal velocity of debris ions, km/s

[1] ESM version 2.12 was the starting point for the DGSM code, now at version 1.4

DGSM_Md: Mass of debris ions, kg
DGSM_fst: Ratio of streaming velocity to thermal velocity
DGSM_AMUd: Average atomic mass of debris ions
DGSM_Zd: Average charge of debris ions
DGSM_Ekf: Kinetic fraction of yield
DGSM_tmax: Maximum time in simulation, t_{max}
DGSM_sfN: Fraction of debris ions that stream N
DGSM_fb: Fraction of debris ions that remain in burst region after t_{burst}
DGSM_fb2: Fraction of debris ions that mirror
DGSM_Frup: Jetting factor
DGSM_Nx: Number of cells in x (eastward) direction
DGSM_Ny: Number of cells in y (radial) direction
DGSM_nFieldCells: Number of cells in z (field line) direction
DGSM_h1: Atmosphere scale height in region 1, km
DGSM_h2: Atmosphere scale height in region 2, km
DGSM_h3: Atmosphere scale height in region 3, km
DGSM_hc: Low altitude cutoff, km
DGSM_hd: High altitude cutoff, km
DGSM_n0: Atmosphere density, amu/cm^3

2.1 Burst Properties

Four parameters describe the explosion and impact the subsequent formation of the initial burst confinement region: the yield Y_B (**DGSM_Yb**), height of burst (HOB) h_B (**DGSM_GeodHeight**), latitude of burst (**DGSM_GeodLat**) and total debris mass (all debris, not just fission fragments) M_d (**DGSM_Md**). The debris mass is correlated with the thermal velocity of the debris U_d (**DGSM_Ud**) through conservation of kinetic energy and only one of these parameters needs to be specified - the other, set to zero in the input file, will be calculated. In this analysis, the velocity was specified and M_d calculated assuming an energy of 4.184 J/kT and that 25% of the yield is converted into kinetic energy for bursts above an altitude of 150 km [4]. The HOB is required to be greater than 100 km, since collisional processes that can occur in the atmosphere and couple to the burst confinement size are ignored. The suggested high-altitude limit from [4] is 8,000 km, as it is not certain whether the magnetic confinement model is valid for extremely high-altitude events. The physics models describing the burst confinement region are valid for altitudes between 200–800 km [5]. However, the DGSM can still be used as a toy model to estimate effects for altitudes greater than ∼800 km, as no other models currently exist. The minimum and maximum altitudes run in these case studies was 500 km and 10,000 km, respectively.

2.2 Atmosphere Properties

The last six parameters define the properties of the ionosphere, which is split into three regions. These parameters were set based on atmospheric density measurements during Starfish: **DGSM_h1** = 10, **DGSM_h2** = 20, **DGSM_h3** = 100, **DGSM_hc** = 180, **DGSM_hd** = 320, and **DGSM_n0** = 4.8×10^6, as derived from [6, 7] and discussed in

[4]. According to [4], these scale heights do not need to be very accurate for altitudes above ~800 km. The parameter **DGSM_AtmGeodHeight** sets the cutoff altitude to which the field lines are traced, thereby setting the lowest altitude grid cells that are considered in the calculations. The cut off altitude used in this work was 80 km. The sensitivity of the results to these atmosphere properties was not studied in this work.

2.3 Grid Definition

The parameters **DGSM_Nx**, **DGSM_Ny**, and **DGSM_nFieldCells** define the spatial grid that is populated for each region when running the code. The extent of the Burst region is calculated in latitude (λ), longitude (ϕ), and L-shell (L), as shown in Fig. 2.1. The radial extent of the Burst region (L_{min}, L_{max}) is calculated from the smaller of the plasma equal mass radius and the magnetic confinement radius. Below ~800 km the equal mass radius is larger and generally asymmetric in the upward and downward direction. For high altitude where the magnetic confinement radius dominates, L_{min} and L_{max} are calculated assuming the Burst region extends from 0.5 – 1.5 times the magnetic confinement radius. The λ and ϕ extent of the Burst region are also calculated from the smaller of the equal radius and magnetic confinement radius, with the addition of a characteristic debris ion gyroradius. With the extent of the Burst region defined, it is divided into cells using the specified Nx and Ny values.

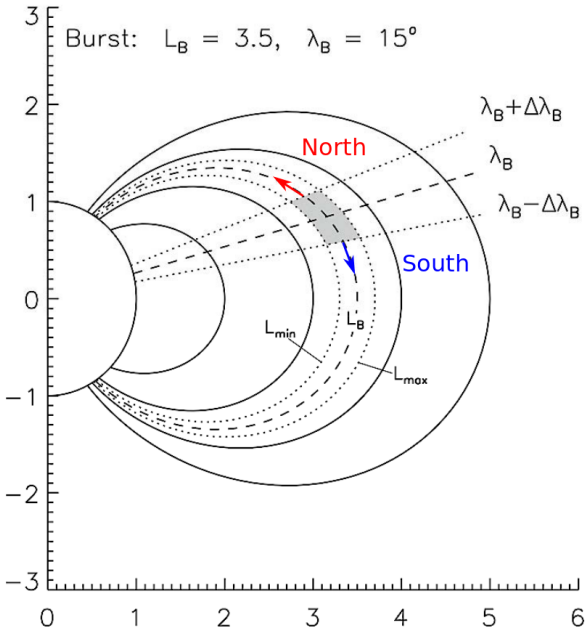

Figure 2.1: Example from [4] showing Burst region (shaded). Debris ions then stream along field lines towards the North (red) and South (blue) regions within the L_{min} and L_{max} regions.

North and South regions are then defined (also shown in Fig. 2.1), which describe the ions streaming along the magnetic field lines away from the Burst region towards the North and South regions until they hit the atmosphere cutoff defined by **DGSM_AtmGeodHeight**. The ions stream as a group, effectively populating the field lines as a moving point source. The streaming velocity is set to a fraction of the debris thermal velocity by **DGSM_fst**. The initial point for these cells are the "top" ($\lambda_B + \Delta\lambda_B$) and "bottom" ($\lambda_B - \Delta\lambda_B$) of the Burst region grid cells. The number of steps along the field line from the initial burst point to the top of the atmosphere is $nFieldCells$. One modification made to the original ESM code as implemented in the DGSM was to make these steps logarithmically spaced to provide better sampling of the DG production time profile at small times. Currently the centered dipole magnetic field model is used. The field line tracing is done using the LANL GeoMag library.

2.4 Number of Fissions

In the DGSM the number of fissions and time step is calculated and reported for each cell. The first step is to calculate the total number of fission debris ions generated in the burst. This is calculated from the yield by first converting the yield in kT to energy in MeV using the conversion factor 2.61×10^{25} MeV/kT. The total number of fissions is then calculated using the average energy release per fission (MeV/fission), which depends on the isotope and taken from [1]. In this work the conversion constant for ^{235}U was assumed.

- ^{235}U: 197.6 MeV/fission
- ^{238}U: 199.7 MeV/fission
- ^{239}Pu: 201.8 MeV/fission

The confinement time of the debris ions within the Burst region before they can stream North/South (t_B) is defined by the Burst region radius and the debris thermal velocity U_d. Debris ions are confined to the Burst region for $t < t_B$, where all cells have a time step with $t_1 = 0$ and $t_2 = t_B$. Debris ions can then remain in the Burst region after t_B through t_{max}, where t_{max} is the maximum time the DGSM will run to and is set by the input parameter **DGSM_tmax**. In this work t_{max} was set to 3000 seconds, corresponding to the duration of data available on delayed gamma production discussed in Section 3.1. The fraction of debris ions that remain in the Burst region after t_B is set by **DGSM_fb**. In the North and South regions each grid cell has a time step associated with it that includes a t_1 entry time and a t_2 exit time based on the debris streaming velocity. In this work the streaming velocity fraction was set to 0.2 based on measurements from Starfish [3, 4]. Ions start streaming after t_B, with the fraction streaming North set by **DGSM_sfN**. Once the ions hit the atmosphere they are either "lost" (no longer tracked) or can mirror along the field line until t_{max}. The fraction of debris ions that will mirror is set by the parameter **DGSM_fb2**. In the case of mirroring an additional number of ions corresponding to t_B to t_{max} is calculated. In this work all debris ions were assumed to leave the Burst region ($fb = 0$), no ions streamed ($fb2 = 0$), and the streaming was equal to the North and South regions ($sfN = 0.5$).

Note that in addition to the total number of fissions in each cell, the number of delayed gammas and number of delayed gammas per second are also reported. These values are calculated using the number of ions and time information of each cell similar to the procedure outlined in Section 3.1. These values can be used with an earlier version of the python code for analysis, however, the current version calculates these values within the python code. This allows for more flexibility in the time-dependence model used for DG production and allows for the future implementation of energy dependence.

3 Python Code

3.1 Delayed Gamma Production

The energy-integrated intensity (# of photons/second/fission) of delayed gammas as a function of time after fission for the isotopes ^{235}U, ^{238}U, and ^{239}Pu used in the current work is

from Foster [8] and shown in Fig. 3.1a. The current approach of DIORAMA [1] is used, where 14 discrete points from 0.01 and 3000 seconds after fission are sampled from this curve. The intensity values used are taken as the average between the fission and 14 MeV intensities. The Foster data start 0.1 seconds after fission; the 0.01 second data point in DIORAMA is an extrapolation from the Foster curve. The 14 discrete points are shown in Fig. 3.1b along with the interpolated values determined by a simple linear interpolation in log-log space. The discrete data points are given in Table 3.1.

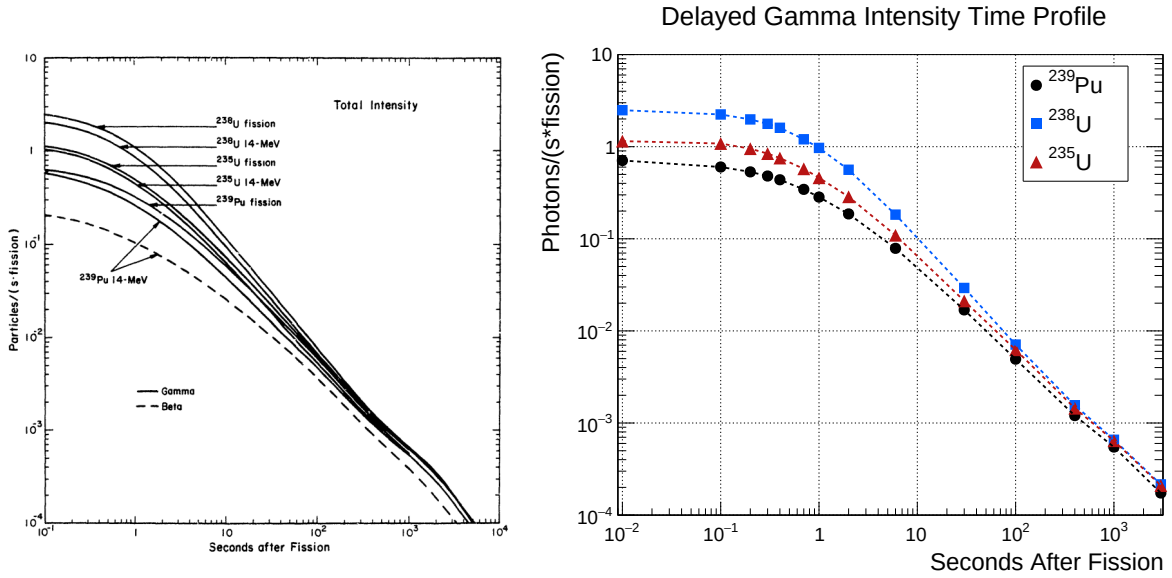

(a) Data from [8].

(b) Discrete points and interpolation used in this work.

Figure 3.1: Total delayed gamma production (# of photons/second/fission) as a function of time after fission.

The values of t_1, t_2, and total number of fissions N associated with each grid cell are used to calculate the total number of delayed gammas produced in each cell. In this work the values for ^{235}U were used to sample the Foster DG production time profile. The DG flux profile is sampled at the mid-point of $log(t_1)$ and $log(t_2)$ using an interpolator to determine the number of photons/second/fission. This number is then multiplied by the width of the time bin $\Delta t = t_2 - t_1$ and the number of fissions N to get the total number of delayed gammas produced in that cell. Two approximations are written into the interpolator function. First, when the Burst region is sampled $t_1 = 0$, which is below the range of the discrete data points used for the interpolation. In this case, Δt is still calculated assuming $t_1 = 0$ but the number of photons/second/fission is approximated after setting $t_1 = 0.01$ seconds. Second, in some cases t_{burst} is less than 0.01 seconds, the minimum value of the discrete data points used for the interpolation. In these few case (low altitude, high debris velocity U_d), the flux below 0.01 seconds is approximated by assigning a DG flux corresponding to the lowest interpolation bin. The effect of these approximations is extremely small.

Table 3.1: 14 discrete data points in this work to parameterize the production of delayed gammas. Units are # of photons/second/fission.

Time (s)	^{239}Pu	^{238}U	^{235}U
0.01	0.7079	2.4912	1.1493
0.1	0.6017	2.2381	1.0824
0.2	0.5328	1.9775	0.9514
0.3	0.4803	1.7719	0.8414
0.4	0.4375	1.6040	0.7527
0.7	0.3441	1.2035	0.5753
1	0.2837	0.9700	0.4598
2	0.1862	0.5618	0.2859
6	0.0788	0.1829	0.1093
30	0.0169	0.0293	0.0212
100	0.00493	0.00711	0.00624
400	0.00120	0.00156	0.00145
1000	0.00055	0.00066	0.00064
3000	0.00017	0.00022	0.00021

3.2 Transport to GEO

The reported position of each cell is used to check the line of sight to the satellite location, using the same algorithm as DIORAMA. Since these events are above the atmosphere, DGs produced in each cell with line of sight are propagated assuming speed-of-light travel and a $1/(4\pi R^2)$ geometric factor that converts the flux into photons/cm^2 at the satellite. No atmospheric transport effects are included at this time, and therefore this code should only be used for events where the full Burst region is above an altitude where these effects become important ($\sim$80–100 km). When the debris ions reach the end of the field line tracing (corresponding to the atmosphere cutoff, 80 km in this study), they continue to emit DGs from that position. Time histograms at the satellite corresponding to the total delayed gamma counts per cm^2 and delayed gammas per second per cm^2 are incremented with each entry in each region. Two histogram regions are created and appended together after looping through all cells. The first region is for the Burst region cells, which covers times up to t_{burst}. The second region is for the North and South region cells, which covers time from t_{burst} to t_{max} or some other desired maximum integration time.

The code also produces time histograms at the satellite corresponding to a point-source assumption, following the discrete data points implemented in DIORAMA, for comparison.

4 Results

Two case studies were run to study how different parameters affect the DG time signature at a GEO satellite. The first case study had a fixed yield but varied the debris velocity for different altitudes and latitudes of burst. The second case study had a fixed altitude of burst and debris velocity but varied the yield and latitude of burst. All other parameters remained constant. The longitude of the burst and satellite were 0° and the satellite altitude and latitude 35786 km and 0°, respectively. In addition to qualitatively comparing the time signature, two proxies for yield were considered and ratios of the results from the higher-fidelity DGSM transport model to the DIORAMA point-source model are presented. The first yield proxy is an integration of the total DG counts at the satellite. This integration is performed from the beginning of the DG signal upon arrival at the satellite to maximum times of 30, 60, 100, and 300 seconds. The second yield proxy uses the amplitude parameter determined in a $t^{-1.2}$ fit [3] to the differential time profile. The same maximum times were used, however, the fit started at $t = 3$ seconds in order to avoid fitting artifacts due to gaps between the counts reported from the Burst and North/South regions. The largest t_B in all cases studies was 2.6 seconds (10,000 km altitude, 0° latitude, 500 km/s debris velocity).

4.1 Debris Velocity Case Study

The debris velocity parameter (**DGSM_Ud**) was varied from 500 km/s to 5,000 km/s, bounding the 2000 km/s measured in Starfish [3, 4]. The streaming velocity was set to 20% of this value also based on Starfish measurements [3]. Four altitudes and two latitudes of burst were considered: 500 km, 1,000 km, 5,000 km, and 10,000 km altitude, and 0° and 60°N latitude. The yield was fixed at 10 kT, corresponding to 1.32×10^{24} fissions.

4.1.1 Comparison of time profile

Figure 4.1 shows the time profile of delayed gammas at the GEO sensor faceplate for a 0° latitude burst at the four different altitudes. The low-altitude bursts (500 km, 1,000 km) show little difference between the point-source model and higher-fidelity DGSM transport model. At higher altitudes, the effects of the large difference in $1/R^2$ that can occur due to the transport is evident. At early times the asymmetric extended Burst region and the initial transport along the field lines leads to DGs being produced closer to the satellite thus resulting in higher flux. At later times the DG flux is lower due to a reduced geometric factor resulting from transport of ions to lower altitudes. Even with the continued production of DGs by debris ions trapped in the atmosphere, the flux at the satellite is below the point-source model for the 5,000 km and 10,000 km bursts. For the 5,000 km and 10,000 km altitude bursts the difference in $1/(4\pi R^2)$ between the HOB and the location of the debris ions trapped in the atmosphere is >25% and >48%, respectively. There is some dependence on thermal debris velocity, and hence streaming velocity, and how quickly the ions are transported down to the atmosphere.

Figure 4.2 shows the time profile of delayed gammas at the GEO sensor faceplate for a 60°N latitude burst at the four different altitudes. An additional effect for high-latitude bursts is observed which is due to the change in geometric factor due to the transport of ions

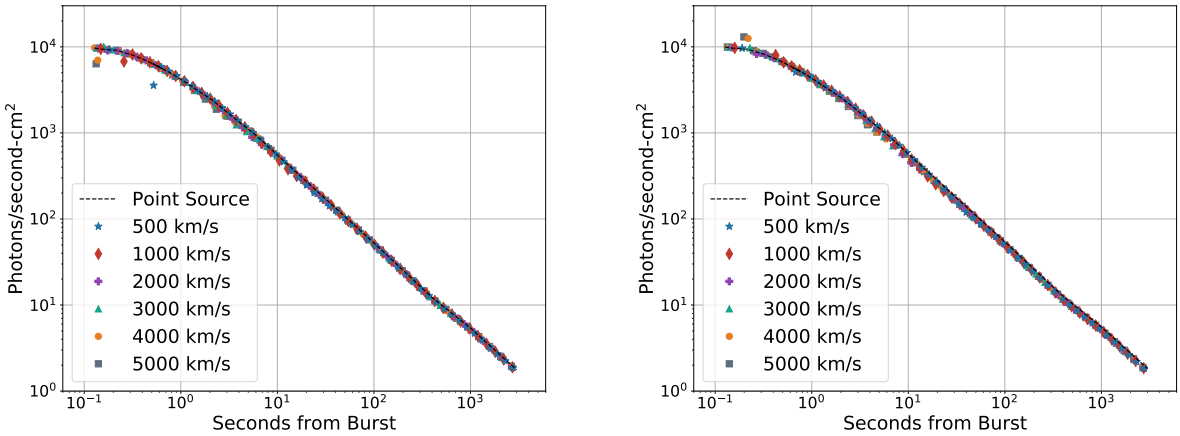

(a) 500 km altitude

(b) 1,000 km altitude

(c) 5,000 km altitude

(d) 10,000 km altitude

Figure 4.1: DG time profile at GEO sensor faceplate for a 10 kT 0° latitude burst at varying altitudes comparing the higher-fidelity transport model to the point-source model. Velocities indicated are thermal debris velocity; the streaming velocity is 20% of these values.

along the field lines at constant L-shell to altitudes closer to, and sometimes even to altitudes past, GEO. This "bump effect" is larger at low altitude and smaller at high altitude, and the location in time strongly dependent on streaming velocity. The bump would also be larger if a larger fraction of debris ions (instead of 50%) streamed to the South. If debris ions were allowed to mirror, this bump above the point-source model would reoccur periodically. Since the central dipole field was used in this study, this effect is expected to be symmetric about the equator.

To better visualize this effect, Fig. 4.3 shows 3D views of the number of delayed gammas per second being produced within grid cells at different times during the transport for a 10 kT, 5,000 km altitude, 60°N latitude burst with a thermal debris velocity of 2,000 km/s (+ points in Fig. 4.2c). Figure 4.3a shows DG production when the debris ions are confined to the Burst region ($t < t_B$) while Figs. 4.3b, 4.3c, and 4.3d show the DG production during transport along the field lines after t_B but before the bump, near the peak of the bump, and

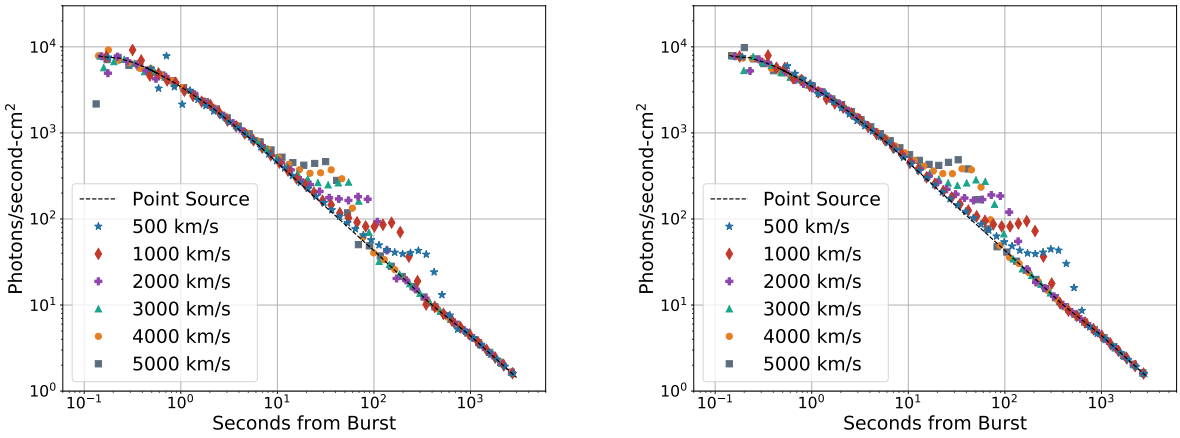

(a) 500 km altitude

(b) 1,000 km altitude

(c) 5,000 km altitude

(d) 10,000 km altitude

Figure 4.2: DG time profile at GEO sensor faceplate for a 10 kT 60°N latitude burst at varying altitudes comparing the higher-fidelity transport model to the point-source model. Velocities indicated are thermal debris velocity; the streaming velocity is 20% of these values.

after the bump, respectively. During initial streaming after t_B (Fig. 4.3b) the production is confined to a fairly small region that is not far from the Burst region. However, at later times (Figs. 4.3c and 4.3d) the debris ions have moved a significant distance from the Burst region and intersect GEO near the peak of the bump, leading to the higher flux observed during this period of the transport.

4.1.2 Yield proxies

The ratio of the yield proxy calculated using the integration method for the higher-fidelity DGSM model to the point-source model is shown in Figs. 4.4 and 4.5 for 0° and 60°N bursts, respectively. For the 0° burst case study, the 500 km and 1,000 km cases do not dependent strongly on thermal debris velocity, and hence streaming velocity, and have a ratio between 0.9–1. The higher altitude cases are more sensitive to the $1/R^2$ effect, and both trend to a larger ratio at smaller streaming velocity as it takes longer for the debris

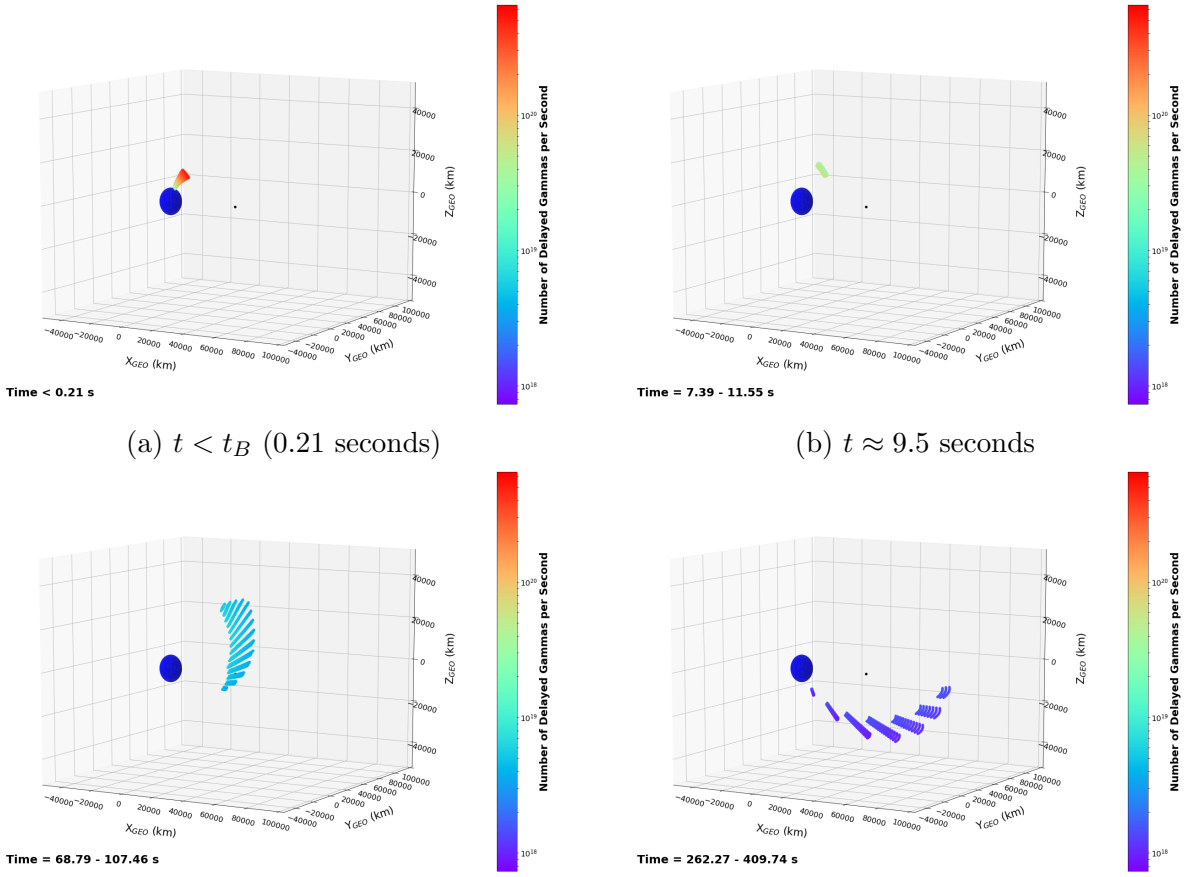

(a) $t < t_B$ (0.21 seconds)

(b) $t \approx 9.5$ seconds

(c) $t \approx 88$ seconds

(d) $t \approx 336$ seconds

Figure 4.3: 3D views of the number of delayed gammas per second being produced within cells during transport for a 10 kT, 5,000 km altitude, 60°N burst with a thermal velocity of 2,000 km/s (streaming velocity of 400 km/s). The large blue sphere represents Earth and the small black dot a GEO satellite at 0° longitude.

ions to be transported from altitudes closer to GEO than the burst altitude and down to the atmosphere. The largest effect seen is a ratio of ∼1.4 for a 10,000 km altitude burst with a 500 km/s debris velocity (100 km/s streaming velocity) using a 30 second integration window. For the 5,000 km and 10,000 km altitude bursts as the velocity increases the ratio decreases, and is ∼0.8 for both at a 300 second integration window and 5,000 km/s debris velocity (1000 km/s streaming velocity). For the 60°N burst case study, the ratio depends on the maximum integration time and the location of the bump for all altitudes. The ratio is generally larger than the ratio at 0°, with the exception of the 10,000 km burst which has a generally smaller ratio at this latitude. The largest effects are seen with 60 second and 100 second integration times; at a 300 second integration time the ratio is fairly flat with velocity with values between 1.3–1.4 for the three lower altitudes.

The ratio of the yield proxy calculated using the amplitude of a $t^{-1.2}$ fit is shown in Fig. 4.6 assuming a fit from 3–60 seconds. It was found that this yield proxy is not very sensitive to the maximum integration time; the fit amplitude is largely fixed by the high flux

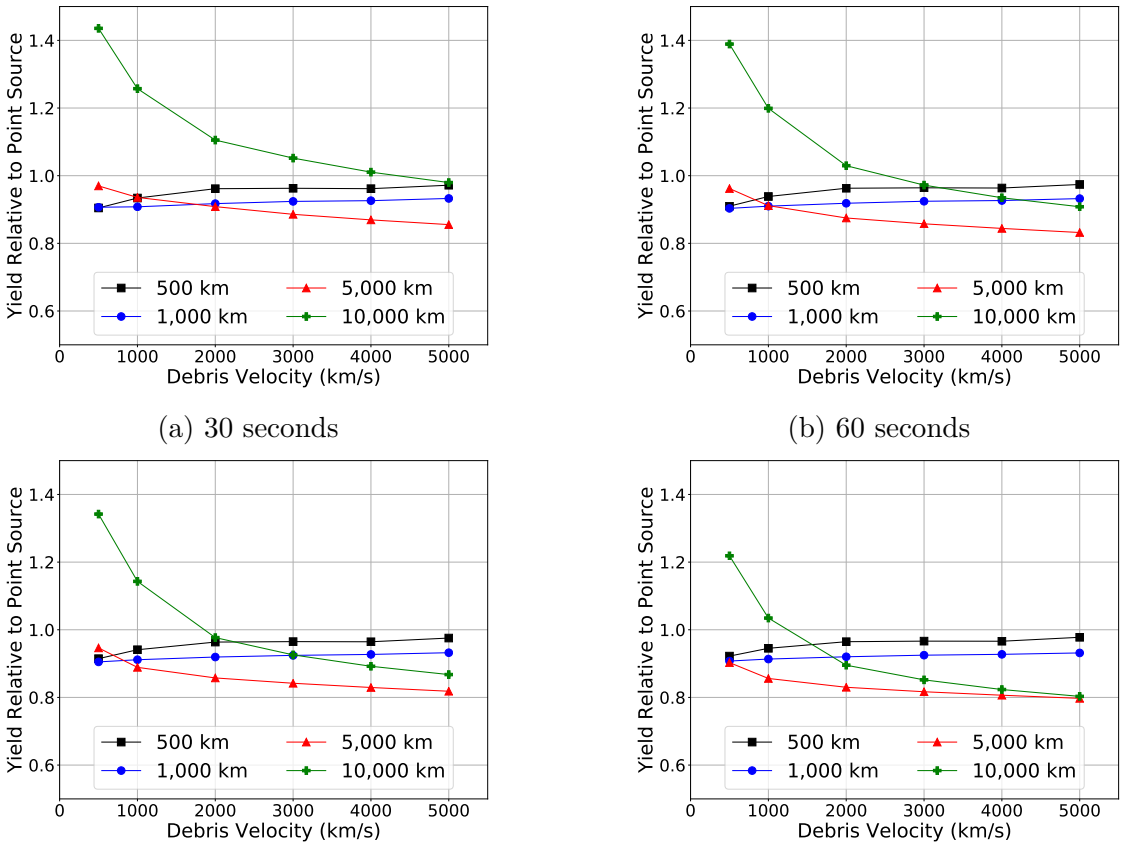

(a) 30 seconds

(b) 60 seconds

(c) 100 seconds

(d) 300 seconds

Figure 4.4: Ratio of yield proxy versus thermal debris velocity calculated by integrating the total DG signal at the satellite for the DGSM model to the point-source model, for different integration times, for a 10 kT 0° latitude burst at varying altitudes.

at early time, before the bump in the high-latitude spectra that occurs at later times. There is some dependence on debris and streaming velocity, with a negative slope with velocity for the 0° latitude burst (Fig. 4.6a) and a positive slope with velocity for the 60°N latitude burst (Fig. 4.6b). For the 0° latitude burst, the ratio from this method is worse for the higher altitude cases, due again to the geometric effects of a large, extended Burst region at early times. For the 60°N latitude burst, the ratio is very similar for all altitudes.

4.2 Yield Case Study

The sensitivity of the field line transport to yield was also studied. For a given burst in latitude and altitude, the yield will impact the size of the Burst region, time of Burst region confinement, and subsequently when fission ions start streaming out along the field lines to the North and South regions. For this study the altitude was fixed at 5,000 km and the thermal debris velocity set to 2,000 km/s (streaming velocity 400 km/s). The yield of the burst was varied from 1 kT (1.32×10^{23} fissions) to 1,000 kT (1.32×10^{26} fissions). At each yield discrete latitudes of 0°, 20°N, 40°N, and 60°N were run.

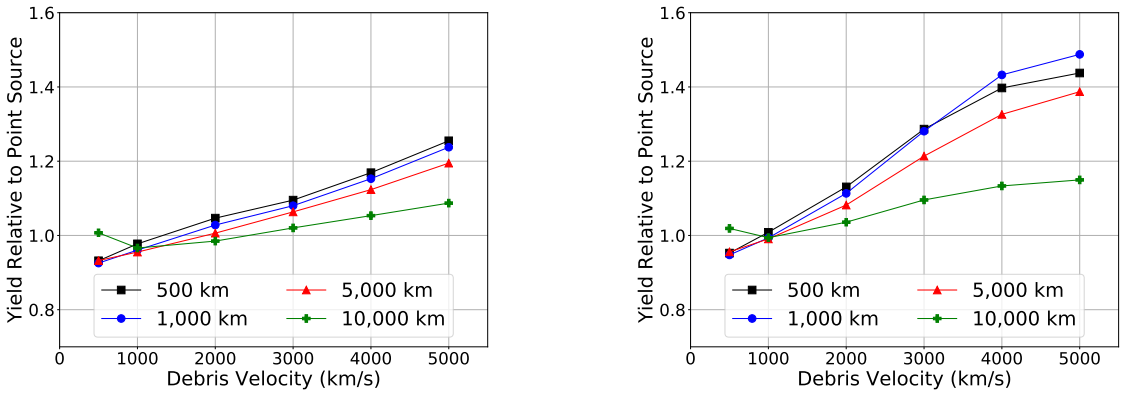

(a) 30 seconds

(b) 60 seconds

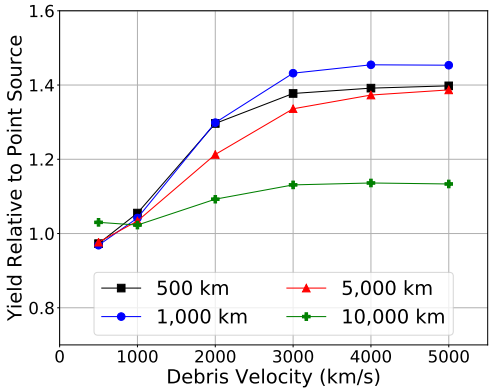

(c) 100 seconds

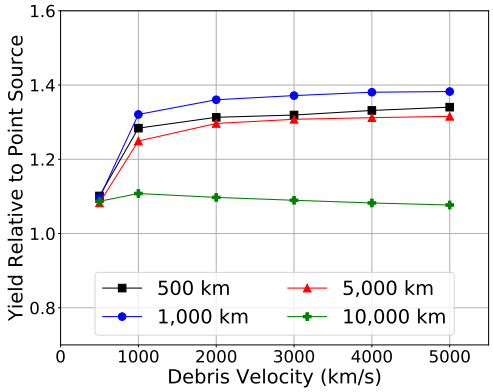

(d) 300 seconds

Figure 4.5: Ratio of yield proxy versus thermal debris velocity calculated by integrating the total DG signal at the satellite for the DGSM model to the point-source model, for different integration times, for a 10 kT 60° latitude burst at varying altitudes.

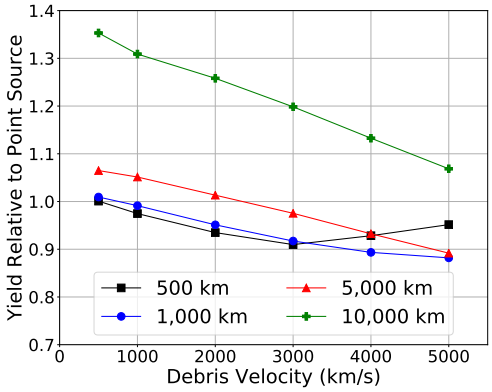

(a) 0° latitude burst

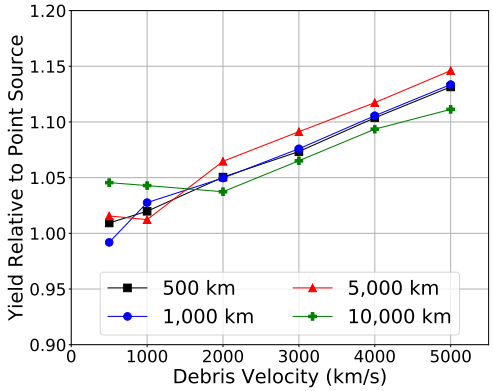

(b) 60° latitude burst

Figure 4.6: Ratio of yield proxy versus thermal debris velocity calculated by a $t^{-1.2}$ fit from 3–60 seconds for the DGSM model to the point-source model, for a 10 kT burst at varying altitudes.

Figure 4.7 shows the relative radial extent of the Burst region from the 5,000 km HOB. At this altitude the Burst region radius is calculated based on the magnetic confinement radius, and is larger in the upward direction (away from the atmosphere) than the downward direction (towards the atmosphere). The size of the Burst region depends on latitude with smaller Burst regions at higher latitude. The higher the yield the larger the Burst region; for a 1 MT burst at 0° latitude, the top of the Burst region is almost a factor of 2 the burst altitude, leading to an increase in the geometric factor at the GEO sensor faceplate of 37%.

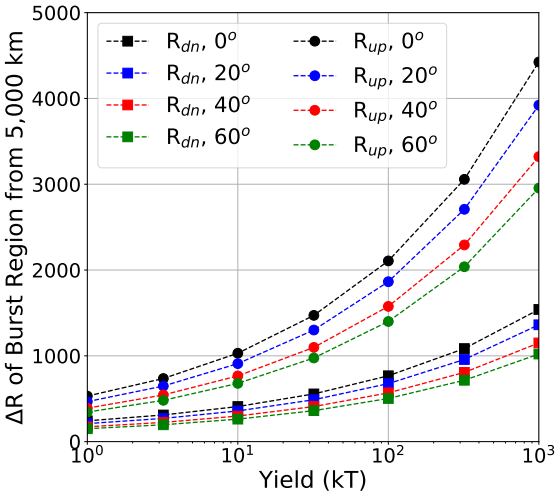

Figure 4.7: Relative radius of the Burst region towards the atmosphere (R_{dn}) and away from the atmosphere (R_{up}).

4.2.1 Comparison of time profile

Figure 4.8 shows the time profile of delayed gammas normalized per kT at the GEO sensor faceplate for 5,000 km altitude bursts of different yield with a thermal debris velocity of 2,000 km/s (streaming velocity of 400 km/s) at the four different latitudes. In general there appears to be very little dependence on yield on the shape of the DG time profile as expected. The exception is that as the yield increases and the Burst region confinement time increases, the start of streaming to the North and South regions increases, seen as an increase in separation between the Burst region histogram (first point) and the North/South region histogram (remaining points). For the three lower latitude cases the $1/R^2$ geometric factor effects of the transport to the atmosphere are observed as a decrease in the DG flux at late times relative to point-source model. At this altitude of burst, the bump effect is only present for latitudes above 40°N. However, the properties of the bump differ between the 40°N and 60°N cases. At 40°N the bump is broader and has a lower peak amplitude relative to the 60°N case. The DG flux from the higher-fidelity model begins to rise above the point-source model at ∼10 seconds, peaks at ∼70 seconds, and has returned to slightly below the point-source model by ∼100 seconds. In contrast, for 60°N the DG flux from the higher-fidelity model begins to rise above the point-source model at ∼20 seconds, peaks at ∼90 seconds, and returns to agreement with the point-source model by ∼200 seconds.

4.2.2 Yield proxies

The ratio of the yield proxy calculated using the integration method for the higher-fidelity DGSM model to the point-source model is shown in Fig. 4.9. The ratio is generally larger for the 40°N and 60°N latitude cases due to the bump effect, but the ratio for these latitudes is more sensitive to the integration time. The relative ratio between the 40°N and 60°N latitude cases changes depending on integration time due to the characteristics of the bump. For the 0° and 20°N latitude cases the ratio gets slightly worse with increasing integration

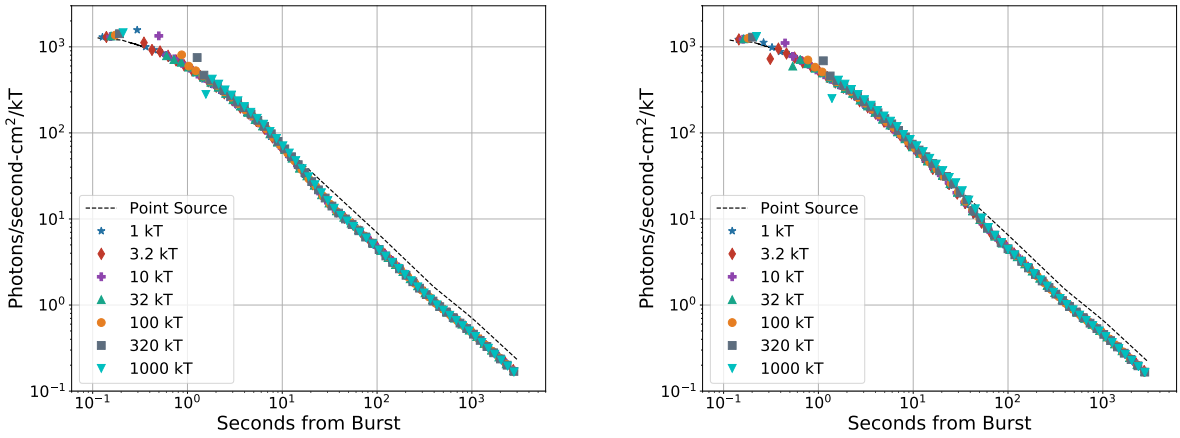

(a) 0° latitude

(b) 20° latitude

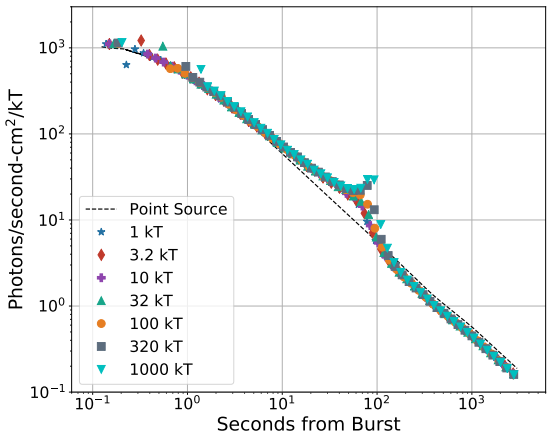

(c) 40° latitude

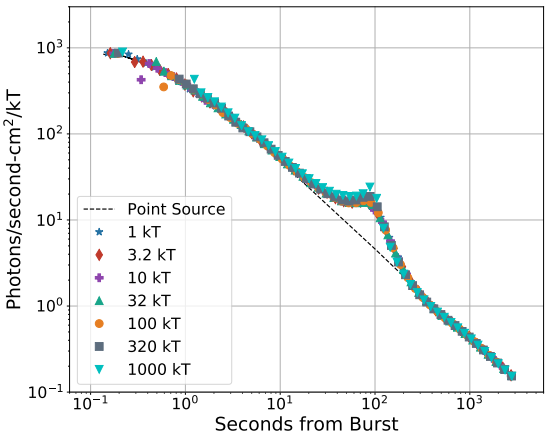

(d) 60° latitude

Figure 4.8: DG time profile at GEO sensor faceplate for a 5,000 km altitude burst with a thermal debris velocity of 2,000 km/s (streaming velocity of 400 km/s) for varying yields and varying latitudes comparing the higher-fidelity transport model to the point-source model.

time, due to the $1/R^2$ geometric effect resulting from the transport of the debris ions down to the atmosphere at later times.

The ratio of the yield proxy calculated using the amplitude of a $t^{-1.2}$ fit is shown in Fig. 4.10 assuming a fit from 3–60 seconds. Again, this yield proxy is not very sensitive to the maximum integration time. In general the ratio increases with yield, but is close to unity and changes only over a small range. The change in the ratio between the highest and lowest yields is larger for the 0° and 20°N latitude cases than the higher latitudes. However, the ratio is generally larger for the 40°N and 60°N latitude cases due to the bump effect.

5 Summary

The Delayed Gamma Source Model and an associated python code were developed to produce the time signature of delayed gammas at a GEO satellite when accounting for debris ion

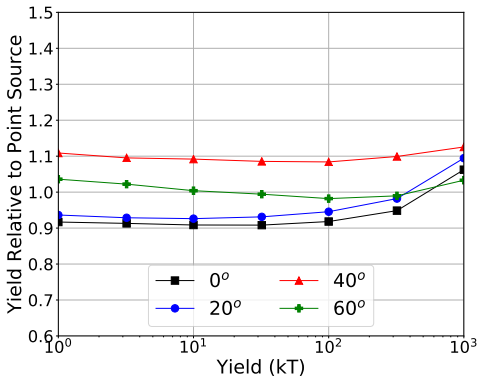

(a) 30 seconds

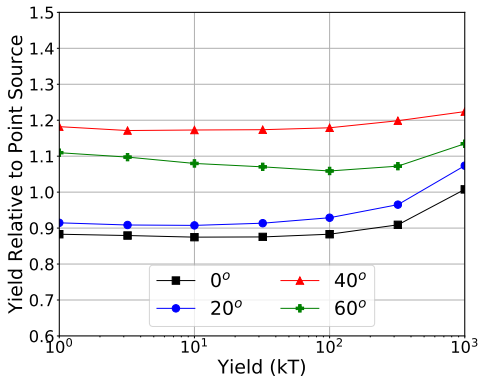

(b) 60 seconds

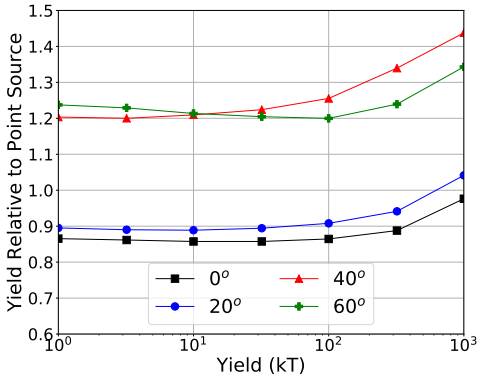

(c) 100 seconds

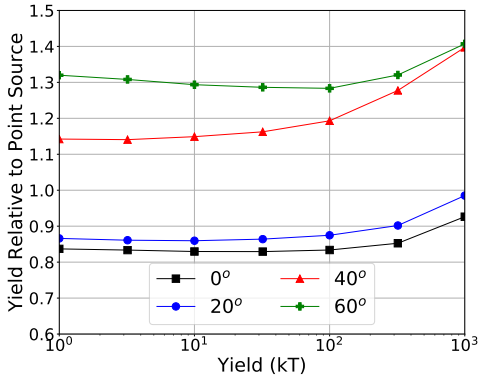

(d) 300 seconds

Figure 4.9: Ratio of yield proxy versus yield calculated by integrating the total DG signal at the satellite for the DGSM model to the point-source model, for different integration times, for a 5,000 km altitude burst with a thermal debris velocity of 2,000 km/s (streaming velocity of 400 km/s) burst at varying yields and latitudes.

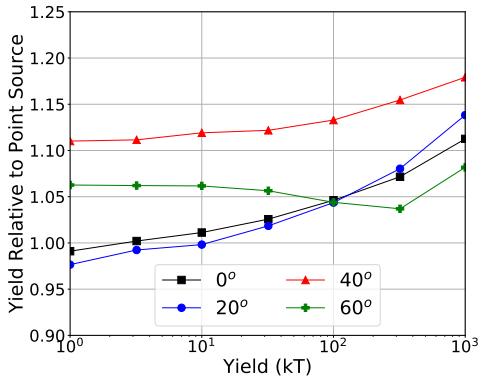

Figure 4.10: Ratio of yield proxy versus yield calculated by a $t^{-1.2}$ fit from 3–60 seconds for the DGSM model to the point-source model, for a 5,000 km altitude burst with a thermal debris velocity of 2,000 km/s (streaming velocity of 400 km/s) burst at varying yields and latitudes.

confinement in an asymmetric extended Burst region followed by field line transport of the debris ions after a high-altitude nuclear explosion. This higher-fidelity model leads to differences in the DG time signature due to the extended spatial distribution of the debris ions and DG production relative to the point-source model that is currently implemented in DIORAMA. These differences are due to changes in the geometric factor resulting from the transport effects, and three qualitative differences between the DGSM model and the point-source model were observed.

1. At early times there can be an increased flux from the higher-fidelity model relative to the point-source model due to the large extended Burst region and initial transport towards the North and South regions; this effect is largest for high altitude and increases with yield.

2. For high-latitude events the transport of debris ions along field lines takes them closer to GEO, resulting in an enhancement in DG counts at the satellite for a short period of time ("bump effect"); this effect is larger at low altitude, increases with latitude, and the characteristics of the bump (time, size) depended on latitude and thermal debris and streaming velocity. The size of the bump would also increase if a larger fraction of ions streamed South (for a North latitude burst), and would reoccur periodically if mirroring on the field lines occurred.

3. At later times, the debris ions are transported to and become trapped in the atmosphere, which can result in a decreased flux from the higher-fidelity model relative to the point-source model; this effect is largest for high-altitude and lower-latitude events. This effect would be enhanced if a larger fraction of ions stream South (for a North latitude burst) and would be reduced if ions mirrored on the field lines instead of becoming trapped in the atmosphere.

In addition to the qualitative comparison of the DG time signature, the ratio of two yield proxies calculated from the DGSM model to the point-source model was presented. The first yield proxy was an integration of the total DG signal at the satellite and the second yield proxy used the amplitude of a $t^{-1.2}$ fit. Overall, the ratio of these yield proxies fell between 0.8–1.5. The dependence of these ratios on altitude, debris velocity, latitude, and yield were presented.

With the groundwork for this improved model complete, future studies and extension to the model can be made. For example, one planned extension for the future is to add energy-dependence of the DG production to the model.

Appendix

DGSM Input File

An example of the DGSM input file.

```
# input parameters for DGSM
#
# outfile run extension
     DGSM__outfile, 10kT_2000Ud_5000km_60deg
#
# Date is yyyymmdd
# Time is in hours (time in seconds/3600) UTC of burst  i.e. 04:41:20 UT
# GeodLat is Deg N. Geodetic latitude of burst
# GeodLong is Deg E.  Geodetic longitude of burst
# GeodHeight is in km.  Geodetic altitude of burst
# Yb is in kt.  Yield of burst
# AtmGeodHeight is in km. Geodetic height of atmosphere cutoff
# haa is in km. Global geodetic height atmosphere cutoff to mimic drift loss cone
# Ud is in km/s.  Thermal velocity of debris ions (set to 0 if want to calculate from Md and energy)
# Md is in kg. Mass of debris ions (set to 0 if want to calculate from Ud and energy)
# fst is ratio of streaming velocity to thermal velocity
# AMUd is in amu. Average Atomic Mass Unit of Debris Ions
# ZD is Average Charge of the Debris Ions
# IDd is the ID of the fission isotope - 0 = 235 U, 1 = 238 U, 2 = 239 Pu
# Ekf is kinetic fraction of yield. If set to 0 then determine from hb.
# tmax is in seconds. Maximum time to use for beta production. 4 hours
# sfN is Fraction of debris that streams to N conj region (after t = tb)
# fb is Fraction of debris ions that remain in the burst region after t = tb (do not stream out);
# fb2 is Fraction of the streaming debris ions that mirror and are not lost to the atm;
# (For only by a "point source" of streaming debris then set fb = fb2 = 0.)
# Frup is Jetting factor
     DGSM__Date, 20160101
     DGSM__Time, 0.
     DGSM__GeodLat,60.
     DGSM__GeodLong,0
     DGSM__GeodHeight, 5000
     DGSM__Yb, 10
     DGSM__AtmGeodHeight, 80.0
     DGSM__haa, 80.
     DGSM__Ud, 3000.0
     DGSM__Md, 0.0
     DGSM__fst, 0.2
     DGSM__AMUd, 50.0
     DGSM__Zd, 2.0
     DGSM_IDd, 0
     DGSM__Ekf, 0.
     DGSM__tmax, 3000.0
     DGSM__sfN, 0.5
     DGSM__fb, 0.0
     DGSM__fb2, 0.0
     DGSM__Frup, 1.0
#
# DEFINE GRIDS AND BINS
```

```
#
#   Nx is Number of cells in x-direction  (points in eastward direction)
#   Ny is Number of cells in y-direction (points in radial direction)
#   nFieldCells is Number of cells in z-direction (points along field line)
#   nPitchAngleBins is Number of alpha bins [0 90]
     DGSM__Nx, 20
     DGSM__Ny, 40
     DGSM__nFieldCells, 80
     DGSM__nPitchAngleBins, 1
#
# DEFINE ATMOSPHERE PARAMETERS
#
#   h1 is in km, Scale height in region 1
#   h2 is in km, Scale height in region 2
#   h3 is in km, Scale height in region 3
#   hc is in km, Low altitude cutoff.
#   hd is in km, High altitude cutoff.
#   n0 is in amu/cm^3. Atm density at Starfish altitude based on Brecht et al 1995 model
#                      & Dyal 2006 paper
     DGSM__h1, 10.0
     DGSM__h2, 20.0
     DGSM__h3, 100.0
     DGSM__hc, 180.0
     DGSM__hd, 320.0
     DGSM__n0, 4.8e6
```

References

[1] A. S. Hoover. *DIORAMA delayed gamma-ray emission*. Los Alamos National Laboratory Report. LA-UR-16-21837, 2016.

[2] S. A. Colgate. "The phenomenology of the mass motion of a high altitude nuclear explosion". In: *Journal of Geophysical Research* 70.13 (1965). URL: https://agupubs.onlinelibrary.wiley.com/doi/abs/10.1029/JZ070i013p03161.

[3] R. G. D'Arcy and S. A. Colgate. "Measurements at the Southern Magnetic Conjugate Region of the Fission Debris from the Starfish Nuclear Detonation". In: *Journal of Geophysical Research* 70.13 (1965). URL: https://agupubs.onlinelibrary.wiley.com/doi/abs/10.1029/JZ070i013p03147.

[4] M. M. Cowee and D. Winske. *HANE Electron Source Model (ESM.V1)*. Los Alamos National Laboratory Report. LA-CP 11-00248, 2011.

[5] Personal communication with Misa Cowee. 2019.

[6] S. H. Brecht, N. T. Gladd, and J. R. Ferrante. *The study of HANE phenomenlogy by kinetic simulations and theory: Debris dynamics, energetic air ion spectrum, and radiation belt dynamics*. Defense Nuclear Agency Technical Report. DNA-TR-95-56, 1995.

[7] P. Dyal. "Particle and field measurements of the Starfish diamagnetic cavity". In: *Journal of Geophysical Research: Space Physics* 111.A12 (2006). URL: https://agupubs.onlinelibrary.wiley.com/doi/abs/10.1029/2006JA011827.

[8] D. G. Foster Jr., T. R. England, and N. L. Whittemore. *Experimental Series Parameters for the Decay of Multigroup Beta and Gamma Spectra from 0.1 to 1000 seconds after a Fission Burst*. Los Alamos National Laboratory/Air Force Weapons Laboratory Report. AFWL-TR-78-4, 1978.

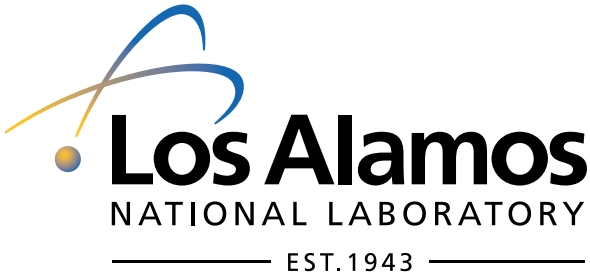

LA-UR-XX-XXXXX